THE JOURNAL OF PHYSICAL CHEMISTRY A

Article

pubs.acs.org/JPCA

Formation of Neutral In_mC_n Clusters under C_{60} Ion Bombardment of Indium

Lars Breuer,[‡] Andrew Kucher,[†] Matthias Herder,[‡] Andreas Wucher,[‡] and Nicholas Winograd*[,†]

[†]Chemistry Department, The Pennsylvania State University, 104 Chemistry Building, University Park, Pennsylvania 16802, United States

[‡]Fachbereich Physik, Universität Duisburg-Essen, 47048 Duisburg, Germany

ABSTRACT: The formation of neutral gas phase indium carbide clusters under C_{60}^+ ion bombardment of solid indium was investigated using laser based postionization prior to mass spectrometric detection. Two different postionization methods were used and shown to provide saturated photoionization efficiency, thereby delivering nearly the same information about the composition of the sputtered material. The resulting size distributions of neutral In_mC_n clusters are compared with those of the corresponding cationic secondary cluster ions and discussed in terms of calculated cluster properties. Investigating the dependence on C_{60}^+ ion fluence, we demonstrate that clusters containing only one carbon atom are formed in single impact events, whereas the formation of more carbon-rich clusters results from carbon accumulation at the bombarded surface.

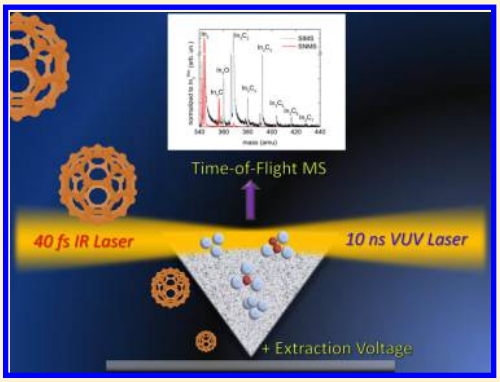

INTRODUCTION

The synthesis of gas phase clusters has had widespread application throughout chemistry.[1] In a recent article, Bernstein et al.[2] investigated the formation of indium carbide cluster ions by bombarding an indium target with an energetic C_{60} ion beam. In earlier work, the same group also found that C_{60} ion bombardment of silver and gold surfaces results in an abundant formation of silver and gold carbide cluster ions.[3] The interesting point of this observation is that these materials do not form stable solid phase carbides. To produce clusters of the form Me_nC_m (Me = Ni, Co, Cu, Bi, Sb, Ag, and Au), gas phase reactions between metal atoms or clusters and hydrocarbon molecules have been applied.[4−15] For the specific case of indium, however, no such experiments had been reported previously. The impetus behind the work of Bernstein et al. was therefore to promote ion sputtering as a method to synthesize novel clusters that are otherwise hard to produce, with the main focus of the paper to investigate the properties of the resulting carbide clusters rather than the mechanism of their production in the course of the sputtering process. The resulting In_mC_n cluster size distribution with respect to n and m was discussed in terms of theoretical calculations of the equilibrium structure as well as electronic properties like binding energy, dissociation energy and ionization energy.[2]

An important aspect of the Bernstein method[2] is the fact that only ionic species could be detected. The formation of these secondary ions in sputtering involves three steps, namely (i) the formation and (ii) the ionization of a "nascent" cluster in the course of the collision-dominated emission event and (iii) the unimolecular decomposition of the intrinsically highly excited nascent clusters during their passage away from the surface. What is detected in such an experiment is those products of the unimolecular fragmentation chain which are metastable on the time scale of the employed detection scheme. Although steps (i) and (ii) are not necessarily decoupled from each other, the important point to note is that the formation of a secondary ion ultimately requires electronic excitation to be involved in the emission process, whereas the formation of a neutral cluster does not. Therefore, the vast majority of particles sputtered from a clean metal surface are emitted in the neutral charge state, thereby rendering the formation of secondary cluster ions the exception rather than the rule. To gain insight into the ion bombardment mediated cluster formation process, it is therefore desirable to complement the information obtained from secondary ions with that obtained from the corresponding secondary neutral species, and this is the goal of the work presented here.

To render them accessible to the experiment, neutral clusters emitted from the surface need to be postionized prior to mass spectrometric detection. For molecular species, two different laser-based strategies have been promoted in an attempt to achieve efficient ionization without extensive fragmentation. In the first approach, single photon ionization (SPI) using nanosecond laser pulses at moderate intensity has been shown to permit the detection of sputtered neutral clusters with ionization efficiencies up to saturation.[16−22] This approach requires VUV laser radiation with a photon energy exceeding the ionization energy of the investigated species and peak

Special Issue: A. W. Castleman, Jr. Festschrift

Received: March 10, 2014
Revised: April 25, 2014
Published: April 29, 2014

dx.doi.org/10.1021/jp5024247 | J. Phys. Chem. A 2014, 118, 8542−8552

intensities of the order of 10^6-10^7 W/cm^2. The second approach involves strong field ionization (SFI) in an intense, ultrashort infrared laser pulse that excerts an electric field of comparable strength to the Coulomb field binding the valence electrons to the nuclei, thereby releasing an electron from the molecule via field emission effects like tunneling or barrier suppression.[23] Using infrared pulses of ∼40 fs duration and peak intensities in the range $10^{13}-10^{15}$ W/cm^2, it has been demonstrated that molecules up to 600 Da can be photoionized with saturation efficiency.[24,25] In the present work, we employ both complementary photoionization schemes to investigate the distribution of neutral clusters formed under bombardment of a sputter cleaned indium surface with a 20 keV C_{60}^+ ion beam. The resulting size distributions are compared to those of the corresponding secondary ions to unravel the effect their ionization process has during cluster formation.

Determining the abundance distribution of neutral clusters in the flux of material released from the surface under ion bombardment requires the investigation of the postionization efficiency. We do this by studying the saturation behavior of the measured signal as a function of the laser intensity and will show that complete ionization efficiency can be achieved for both employed postionization methods without excessive fragmentation of the sputtered clusters. To enable a quantitative comparison between neutral and ionized species, we then investigate the fraction of sputtered particles that is intercepted by the postionization laser. The results will then be used to determine the ion fraction, i.e., the probability that a sputtered particle is emitted in a charged state, i.e., as a secondary ion. We will show that the vast majority of the sputtered material is emitted in the neutral state, with nearly negligible ion fraction for all In_mC_n clusters investigated here.

The abundance distributions measured under steady state conditions, i.e., after prolonged C_{60}^+-bombardment, for pure indium and indium carbide clusters will be discussed in terms of electronic cluster properties like ionization energy and dissociation energies for different fragmentation reactions as calculated by Bernstein et al.[2] We will show that the abundance distributions of neutral clusters significantly differ from those of the respective cations, reflecting particularly the differences in cluster stability in light of the unimolecular dissociation accompanying the cluster formation process. Last, but not least, we investigate the role of the C_{60}^+ ion fluence in an attempt to answer the question, whether the observed clusters are formed in single impact events or as a consequence of carbon accumulation at the ion bombarded surface.

EXPERIMENTAL SECTION

The experiments were performed on two virtually identical instruments that have been described in detail elsewhere.[26,27] Both systems utilize a 20 kV C_{60}^+ ion source, delivering a beam current of about 50 pA into a spot size of the order of several μm and a reflectron-type time-of-flight (TOF) mass spectrometer mounted to an ultrahigh vacuum chamber with a base pressure of about 10^{-9} mbar. In addition to the fullerene source, one instrument was equipped with a liquid metal ion source delivering a focused 25 keV Gold (Au^+, Au_2^+, and Au_3^+) ion beam of about 10 nA into a spot size of the order of 1 μm. All ion beams were directed to the surface of a clean indium sample under an incidence angle of 45° and operated in a pulsed mode with a pulse length of about 2000 ns. During the primary ion pulse, the sample was held at ground potential, thereby keeping the space above the surface field free. Secondary ions as well as sputtered neutral particles ejected from the surface as a consequence of the ion bombardment were therefore allowed to expand freely according to their emission angle and velocity distribution, before they were interrogated by means of an extraction field that was switched on shortly (∼10 ns) after the end of the primary ion pulse. At the start of the extraction pulse, secondary ions that are present in the space between surface and extraction electrode are accelerated into the TOF spectrometer and focused onto a microchannelplate detector. The postionization laser beam is directed parallel to the surface at a distance ("height") of 0.5−1 mm and fired shortly (∼75 ns) after the start of the extraction pulse. The delay is introduced to separate the flight time peaks arising from secondary ions and postionized neutrals, because the flight time zero for the secondary ions is determined by the extraction field, whereas that for the photoions is determined by the laser pulse. Apart from this difference, the spectrometer does not distinguish between secondary ions and postionized neutrals, thus enabling the detection of both species under otherwise identical experimental conditions. These facts will be important in the discussion below.

The sample used in these experiments consists of a polycrystalline indium foil that was mounted to an *xyz*-translation stage. To ensure reproducible surface conditions, the initial surface contamination was removed by prolonged ion bombardment to a fluence of the order of 10^{16} cm^{-2} using a dc beam rastered over an area of 400 × 400 μm^2. During one set of experiments, this was done using the C_{60}^+ beam operated in dc mode, thereby ensuring the establishment of steady state sputtering conditions before taking data using the same beam, now operated in pulsed and spot mode and centered within the prebombarded area. In a second set of experiments, the surface was prebombarded using a dc gold ion beam rastered over an area of 700 × 700 μm^2, with the goal of completely removing any carbon contamination that may have been present at the virgin indium surface. The gold bombardment was continued until no carbide clusters were detectable in the mass spectrum. Note that the surface prepared in this manner did have gold atoms incorporated, leading to the observation of abundant indium−gold clusters in the sputtered flux which, however, were disregarded in the present work. The surface was then analyzed with the C_{60}^+ beam using alternating ion bombardment and data acquisition cycles to determine the role of possible carbon accumulation in the surface. During a bombardment cycle, the C_{60} beam was operated in dc mode and rastered over an area of 400 × 400 μm centered within the gold prebombarded area, thereby applying a fluence of about 7 × 10^{11} cm^{-2} per cycle.

The postionization laser used in instrument 1 was an F_2 excimer laser (Coherent Excistar XS 500) delivering pulses of up to ∼2 mJ energy and 10 ns duration at a wavelength of 157 nm. The corresponding photon energy of 7.88 eV is above the ionization energy of indium atoms (5.79 eV) as well as all indium[28,29] and indium carbide[2] clusters and therefore should allow nonresonant single photon ionization (SPI) of all neutral species investigated here. The VUV beam was introduced into the TOF spectrometer via an evacuated beamline and a spherical CaF_2 lens of 150 mm focal length, which simultaneously served as a window separating the beamline from the ultrahigh vacuum chamber. To control the position of the laser focus with respect to the sensitive volume of the mass spectrometer, the lens was mounted on an *xyz*-manipulator that was firmly connected to the UHV chamber. In such a manner,

dx.doi.org/10.1021/jp5024247 | J. Phys. Chem. A 2014, 118, 8542−8552

both the vertical distance ("height") and the lateral position of the laser focus with respect to the ion optical axis of the TOF spectrometer could be precisely controlled by moving the lens in the *y*- or *x*-axis, respectively. When the lens was translated along the *z*-axis (the propagation direction of the laser), the focal diameter of the beam in the sensitive volume from which ions are being extracted and transmitted through the TOF spectrometer could be varied between ∼100 μm and ∼1 mm. In some experiments, the extension of the sensitive volume was restricted to match the effective laser beam width by introducing a 1 mm diameter aperture in front of the entrance electrode of the TOF spectrometer. The laser output was varied and regulated via the discharge high voltage and measured using the internal energy monitor, which was calibrated using a GenTec power meter. In addition to the "external" measurement, the laser pulses entering the vacuum chamber were monitored using a two-grid photoelectric detector described elsewhere.[30]

In instrument 2, postionization of the sputtered neutrals is accomplished by means of a laser delivering intense, ultrashort pulses at near-infrared wavelengths between 1160 and 2580 nm. The system employed in these experiments (Coherent Legend Elite Duo) produces pulses of 10 mJ energy, 40 fs duration, at a wavelength of 800 nm and a repetition rate of 1 kHz. Its pulse width is checked by frequency resolved optical gating in the Swamp Optics Grenouille 8-20-USB. The laser output is used to pump an optical parametric amplifier (OPA) (Light Conversion TOPAS-C-HE), the output wavelength of which is tunable in the 1160−2580 nm range, with a combined signal and idler conversion efficiency between 30% and 40% of the pump power. The output intensity is adjusted by changing the delay between the pump and seed pulses in the second amplification stage of the OPA, because this method has almost no effect on the output wavelength and pulse width. The signal and idler outputs of the OPA are filtered with appropriate dichroic mirrors. The generated wavelengths are confirmed by detecting their frequency doubled light in an Ocean Optics USB 4000 spectrometer. The beam is focused into the mass spectrometer using a 150 mm (at 587.6 nm) focal length lens, which produces a 75 ± 25 μm focal diameter for all wavelengths. Under these conditions, the Rayleigh range of the laser focus is about 1 mm, which is comparable to the extension of the sensitive volume of the mass spectrometer. Therefore, in some of the experiments, ion collection was restricted in the direction of the laser propagation using a 600 μm wide slit aperture placed between the laser focus and the entrance electrode of the TOF spectrometer. The laser power is monitored using a power meter and the intensity is calibrated relative to the known ionization behavior of pure Xe gas, which is introduced into the vacuum chamber via a leak valve.

RESULTS AND DISCUSSION

The main goal of this work is to determine the abundance distribution of neutral clusters in the plume of material sputtered from an indium surface under bombardment with a C_{60}^+ ion beam and compare it with that of the corresponding cationic clusters. This section is therefore organized as follows. First, to facilitate a quantitative comparison, it is necessary to assess the efficiency of the postionization methods used to render the neutral species accessible to detection in the TOF mass spectrometer. We do so by looking at the saturation behavior of the employed photoionization techniques. These schemes are then compared to assess the possible role of laser-induced fragmentation accompanying the photoionization process. Next, we present the size distribution of pure indium neutral and cationic clusters emitted under C_{60}^+ bombardment and compare the results to similar data obtained using atomic projectile ion beams. The measured distributions are discussed in terms of known facts regarding the formation of metal clusters in sputtering. Subsequently, we present the measured abundance distributions of In_mC_n carbide clusters as a function of their stoichiometry (m/n) and size (nuclearity, $m + n$). The results are discussed in terms of relevant cluster properties such as ionization energy, dissociation channels and energies etc. that are taken from the literature. Finally, we investigate the role of C_{60}^+ ion fluence to shed light on the question whether the observed clusters are being formed during single impact events or as a consequence of carbon accumulation at the C_{60}^+ bombarded surface.

Photoionization Efficiency. To obtain quantitative information about the postionization efficiency, we investigate the saturation behavior of the photoionization process in the regime of high laser intensity. For molecular species, the possibility of photon induced fragmentation must also be addressed at least at a semiquantitative level. In principle, the signal detected by a TOF spectrometer as used here is determined by the spatial and temporal overlap between the plume of sputtered particles emitted from the surface, the ionization laser and the sensitive detection volume of the mass spectrometer. Due to the short laser pulses employed here, any motion of the neutral particles during the laser pulse can be neglected and the experiment is therefore sensitive to the number density of neutral particles rather than their flux. The measured signal can in general be described as[31]

$$S = \int n(\vec{r})\, \alpha^0(\vec{r})\, T(\vec{r})\, \mathrm{d}^3 r \tag{1}$$

where n is the number density of neutral target species, α^0 denotes the postionization probability, and T describes the instrument transmission, i.e., the probability that a photoion created at position $\vec{r}$ will be extracted into the TOF spectrometer and detected in the flight time spectrum.

One possible approach to simplify eq 1 is to deliberately defocus the ionization laser, rendering the postionization probability constant across the effective detectable plume determined by the overlap of n and T. To gain further information, it is advantageous to look at the signal of gas phase species that are present in the residual gas and photoionized by the laser. For such species, the number density is constant, the (thermal) starting velocity of the generated photoions is negligible, and the remaining integral over T therefore describes the true sensitive volume of the TOF spectrometer. Sputtered particles, on the other hand, are being emitted from a specific point where the primary ion beam hits the surface and exhibit a relatively broad distribution of emission angles and velocities. As a consequence, n and T are not independent and the effective detectable plume may crucially depend on the parameters of the ion bombardment such as beam energy, impact angle and the location and extension of the ion bombarded surface area.

For a single photon absorption process, the laser intensity required to reach saturation ionization efficiency is relatively small and the laser can be defocused to sample the entire plume. The theoretically expected photoionization probability of a molecule as a function of the laser intensity I_L is given by

dx.doi.org/10.1021/jp5024247 | J. Phys. Chem. A 2014, 118, 8542−8552

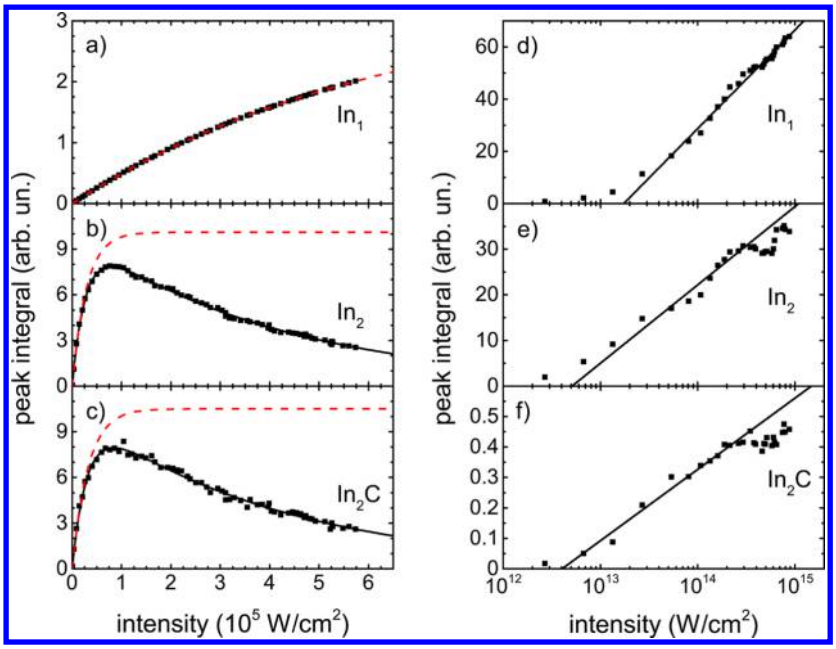

Figure 1. Laser intensity dependence of photoionization signal measured for neutral In atoms, In_2 dimers, and In_2C clusters produced under bombardment of solid indium with 20 keV C_{60}^+ ions using VUV single photon ionization at 157 nm (a, b, c) and strong field IR photoionization at 1200 nm (d, e, f). (See text for details regarding the solid and dashed lines.)

$$\alpha^0(I_L) = \phi_i[1 - \exp(-\sigma_a I_L \tau)] \exp(-\sigma_f I_L \tau) \quad (2)$$

where σ_a is the photoabsorption cross section, ϕ_i is the branching ratio between intact single photon ionization and fragmentation, σ_f denotes the cross section for higher order fragmentation by absorption of further photons, and τ is the laser pulse duration. The laser intensity dependences of the signal measured for In, In_2, and In_2C using a defocused laser beam are shown in Figure 1a. In these experiments, the VUV laser output was varied by means of the discharge voltage and defocused to a focal dimension of about 1×0.5 mm^2 in directions parallel and perpendicular to the surface, respectively. The solid lines represent fits of eq 2 to the data, which describe the measured signal variation very well and deliver the saturated signal S_{sat} as well as the values of σ_a and σ_f as fitting parameters (for indium atoms, σ_f was naturally fixed at zero). The resulting photoionization efficiencies can be obtained by correction for the multiphoton fragmentation term in eq 2 and is depicted as dashed (red) lines in Figure 1a. Comparison with the known photoionization cross section of Mo atoms[31] yields the saturation intensity for the clusters to be around 2×10^5 W/cm^2, whereas that of the indium atoms is by more than an order of magnitude larger. This appears to be a rather common feature in single photon ionization of sputtered clusters which has been found for other metals using the same VUV wavelength employed here[32] as well as for indium atoms and clusters using different laser wavelengths.[18,28]

Under strong field photoionization conditions, on the other hand, a tightly focused laser is used to generate high enough intensity for efficient ionization. In this case, the ionization volume, i.e., the volume effectively sampled by the laser, will depend on the laser intensity and expand with increasing intensity. To investigate the photoionization efficiency under these conditions, the extension of the ionization volume in the direction along the laser beam is restricted to a length l (below the Rayleigh range), as described in the Experimental Section. Assuming a Gaussian beam profile, the saturation behavior of the measured signal is under these "parallel beam" conditions described by[33]

$$\frac{dS}{d(\ln I_0)} = Tn\pi R^2 l \phi_i [1 - \exp(-\int_{-\infty}^{\infty} W(I_L(t))/\phi_i)] \quad (3)$$

where n and T have the same meaning as above, R is the distance from the center of the laser beam where the intensity has fallen to I_0/e, and I_0 is the intensity in the center of the laser beam. In deriving eq 3, use was made of the fact that the laser beam diameter is small compared to the extension of the detectable plume, so that both n and T can be assumed to be constant across the ionization volume. In the limit of high intensity, the photoionization efficiency in square brackets becomes saturated and the signal varies asymptotically as

$$S(I_0) \approx \pi R^2 l \ln\left(\frac{I_0}{I_{sat}}\right) \cdot n \cdot T = \pi R'^2 l \cdot n \cdot T \quad (4)$$

where $\pi R'^2 l$ denotes the ionization volume, i.e., the volume where $I_L > I_{sat}$. Plotting the signal vs $\log(I_0)$ therefore yields an asymptotic straight line, which can be used to determine the saturation intensity I_{sat} as shown in Figure 1b.[33] Again, we find a lower saturation intensity for the clusters ($\sim 5 \times 10^{12}$ W/cm^2) than for the indium atoms ($\sim 2 \times 10^{13}$ W/cm^2). Once I_{sat} is known, the lateral extension R' of the ionization volume can be calculated for a given laser intensity I_0 using eq 4.

For a quantitative comparison of sputtered neutral cluster yields with those of the corresponding secondary ions, it is important to note that particularly a focused laser might significantly undersample the detectable sputtered plume. In principle, lateral scans of the laser beam can be used to address that problem. As a first step, we use the tightly focused laser to map the sensitive volume of the mass spectrometer by following the photoionization signal of gas phase Xe atoms as a function of the laser position. In doing so, the laser beam was positioned for optimum signal and then scanned in directions parallel and perpendicular to the surface, corresponding to the

dx.doi.org/10.1021/jp5024247 | J. Phys. Chem. A 2014, 118, 8542−8552

coordinates orthogonal to and along the ion optical axis of the spectrometer. The result of such scans is shown in Figure 2,

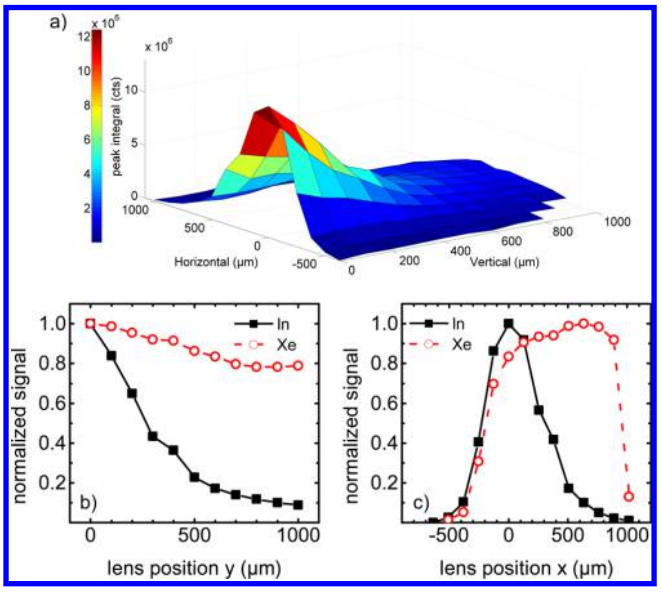

Figure 2. Signal of photoionized gas phase Xe atoms and sputtered neutral In atoms as a function of the position of the ionization laser during strong field photoionization at a wavelength of 1350 nm, peak intensity $I_0 \sim 10^{15}$ W/cm^2 and focal diameter $d \sim 75$ μm ($R \sim 26$ μm): (a) full 2D-signal distribution; (b) vertical scan along the surface normal; (c) horizontal scan parallel to the surface through the position of maximum detected signal.

revealing a lateral extension of the sensitive volume of about 1.5 mm. As expected, the transmission probability is practically constant throughout the entire sensitive volume and drops rapidly at its edge, being determined essentially by the ion optical properties of the mass spectrometer. In the direction along the ion extraction axis, the curve shows an almost constant transmission probability over the scanned interval of about 1.5 mm[a] above the surface. As a second step, we then follow the signal of sputtered neutral species as a function of the laser position to map the detectable sputtered plume as introduced above. The results measured for sputtered In atoms are also shown in Figure 2. It is seen that the sputtered plume is not centered within the sensitive volume. This is presumably due to the fact that the C_{60} ion beam impinges under 45° with respect to the surface normal, rendering the distribution of sputtered particles anisotropic, with particles being prefentially ejected in an off-normal direction.[34] To efficiently sample these, the ion beam needs to be displaced from the ion optical axis of the spectrometer. As a consequence, the neutral particles probed by the photoionization laser possess a starting velocity component orthogonal to the ion optical axis, which needs to be compensated by a lateral displacement of the ionization volume. Note that the same is true for the secondary ions, which follow the same trajectories and are detected in exactly the same manner as the postionized neutrals because the space above the surface is field-free until the extraction field is switched on. In the direction along the ion optical axis, the signal reflects the expected $1/r^2$ decrease in number density, which is expected for a point source of sputtered particles at the surface.

The complete experimentally detectable plume mapped out this way is shown in Figure 2a. These data can now be integrated to estimate the fraction of the entire plume that is being intercepted by the laser being positioned for optimum signal. In doing so, we multiply the signal measured at the maximum in Figure 2a with the sampled area $\pi R'^2$ as calculated above and divide by the sum of all signals shown in Figure 2a, multiplied by the stepping intervals Δx and Δy of the x and y scans. As a result, we find that at a peak intensity of 10^{15} W/cm^2, corresponding to $I_0/I_{sat} = 50$, the laser intercepts about 3% of the sputtered plume. This value can be used to calculate the ion fraction of sputtered indium atoms. In this context, it is important to note that the measured secondary ion signal represents the integral over the entire detectable plume. From the measured signal ratio of 50 between the (undersampled) postionized neutral and the corresponding secondary ion signal, one therefore finds an ion fraction of $\sim 6 \times 10^{-4}$ for the sputtered indium atoms. This value is typical for a sputter cleaned metal surface and is, moreover, in good agreement with that measured by Samartsev et. al[35] for In atoms sputtered under gold cluster bombardment of a clean indium surface.

As a result of the above discussion, we expect the postionization efficiency of all detected clusters to be saturated under both single photon and strong field ionization conditions employed here. To examine this notion, we plot in Figure 3 the

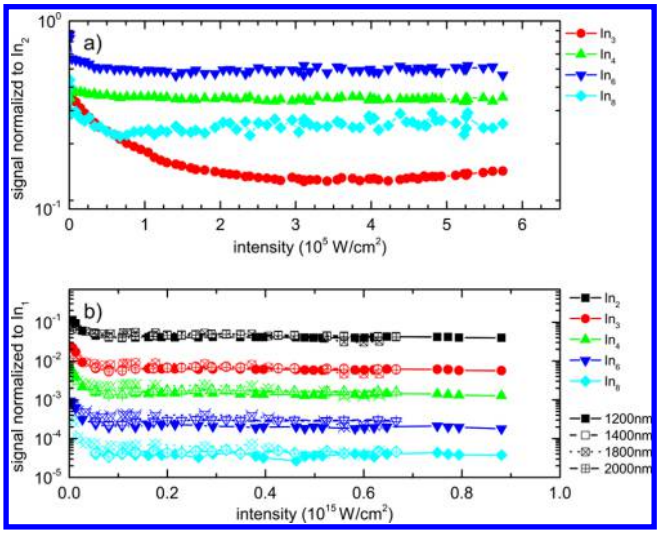

Figure 3. Signal of postionized neutral indium atoms and clusters produced under bombardment of solid indium with 20 keV C_{60}^+ ions normalized to that of In_2 dimers (a) or In atoms (b) vs ionization laser intensity for (a) VUV single photon ionization at 157 nm and (b) IR strong field photoionization at the indicated wavelength.

ratio of the postionization signal measured for a specific cluster to that measured for In atoms. Data obtained under strong field ionization conditions are shown in Figure 3b for different wavelengths of the ionization laser. It is seen that in all cases the ratio first decreases at lower intensities and then becomes constant at intensity values above 10^{14} W/cm^2. The initial decrease is due to the fact that the In atom signal is obviously not entirely saturated below intensities about 5×10^{13} W/cm^2, an observation that fits nicely to the saturation intensity of 2×10^{13} W/cm^2 obtained from Figure 1b and the fact that about e times I_{sat} is needed for complete saturation.[33] What is also evident from the data is that the resulting signal ratio only weakly depends on the particular wavelength used for strong field photoionization.

dx.doi.org/10.1021/jp5024247 | J. Phys. Chem. A 2014, 118, 8542−8552

Under single photon ionization conditions, the available laser intensity is not sufficient to completely reach saturation of the In atom signal (Figure 1a). In this case, we therefore plot the cluster signals relative to that of the In_2 dimer in Figure 3a. Also in this case, it is evident that the signal ratio of different clusters becomes constant once the laser pulse intensity is larger than about 4×10^5 W/cm^2, indicating saturated ionization efficiency for all clusters.

Cluster Size Distribution. Once saturated ionization conditions are established, the measured postionization signals directly represent the density of the respective clusters within the sputtered plume. The resulting size distribution measured for pure indium clusters using the two different postionization strategies is plotted in Figure 4. Because all wavelengths

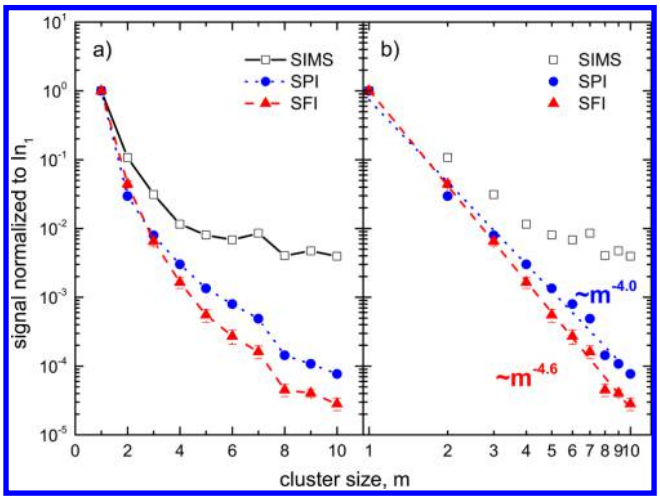

Figure 4. Size distribution of neutral In_m clusters (SPI, blue; SFI, red) and In_m^+ cluster ions (SIMS, black) produced under bombardment of a solid indium surface with 20 keV C_{60}^+ ions plotted in (a) semilog and (b) double-log fashion. The neutral species were postionized using either a VUV single photon ionization (SPI, blue) or a IR strong field photoionization (SFI, red) scheme.

employed during strong field photoionization yield essentially the same result, we include here the data averaged over all used wavelengths (1200, 1400, 1800, and 2000 nm) to reduce the statistical noise. First, and probably most importantly, it is seen that both postionization methods yield very similar size distributions, with the abundance of In_m clusters decreasing monotonically with increasing nuclearity m. This observation has been made before[19] and represents a rather typical feature of the cluster formation process in sputtering.[32] In fact, if the distribution is plotted in a double-log fashion (Figure 4b), one finds a straight line indicating a power law dependence of the cluster yield according to $m^{-\delta}$, with the exponent δ depending on the ion bombardment conditions.[21,36−38] Earlier experiments on different metals under bombardment with atomic projectile ions have revealed the value of δ to be linked to the sputter yield Y, with δ decreasing with increasing Y as long as the sputtering process is governed by a linear collision cascade.[18,36,39]

The situation is different if polyatomic projectiles are used for bombardment, because under these conditions the sputtering process is dominated by a collisional spike. It has been argued that cluster formation under these conditions may lead to nearly constant values of δ independent of the sputter yield.[37,40,41] From the present data, we find δ = 4.0 and 4.6 for the size distributions measured with both postionization techniques. The value of 4.0 agrees with that determined by Staudt et al.[18] (3.9) for bombardment of indium with 15 keV Xe^+ ions using VUV single photon ionization at 193 nm for postionization. Under these conditions, a total of about 14 indium atoms (regardless of bond state) are on average being removed from the surface per projectile impact. It has been argued that the transition between linear collision and spike regimes may be marked by a sputter yield around 20 atoms/impact.[42] For 20 keV C_{60}^+ projectiles, the yield is estimated as ∼150 atoms/impact[43] and the emission process is therefore clearly spike dominated. The fact that similar cluster size distributions are observed under both bombardment conditions therefore nicely corroborates the notion of a constant exponent once the spike regime is reached.

A close inspection of the size distributions in Figure 4 reveals slight differences between both postionization methods. As a trend, larger clusters appear to be less efficiently detected under strong field photoionization than under single photon ionization conditions, while at the same time the dimer signal appears to be slightly enhanced. Both observations are consistent with a higher degree of photofragmentation under SFI conditions. In fact, it appears surprising at first glance that a cluster like In_{10} can be photoionized to saturation efficiency by brute force without being completely fragmented. From the observed signal ratio, one finds that the branching ratio ϕ_i for intact ionization of In_{10} must be by a factor of 3 lower than that under SPI conditions, indicating that about 60% of the neutral In_{10} clusters are being fragmented in the high intensity laser field. However, the effect is less pronounced for smaller clusters and should therefore be negligible for the small indium carbide clusters discussed below.

Another striking observation in Figure 4 concerns the secondary cation cluster distribution, which appear to fall much more slowly with increasing cluster size than the corresponding neutral clusters. However, analysis reveals that this is due to the fact that the data were normalized to the respective monomer signal. Considering the ion fraction of sputtered monomers as discussed above, the curve labeled "SIMS" in Figure 4 must therefore be shifted down by 4 orders of magnitude to facilitate a quantitative comparison. It is evident that practically all indium clusters formed under C_{60}^+ ion bombardment of a clean indium surface are neutral, leaving the secondary ion formation as a minor emission channel in all cases investigated here. However, it is interesting to note that all three distributions plotted in Figure 4 show an exceptional signal drop between In_7 and In_8. This observation has been made before[19] and reflects an enhanced stability of the In_7^+ cluster ion with respect to In_8^+. The fact that the distribution of postionized neutral clusters exhibits the same intensity drop therefore indicates that this feature must be induced by photofragmentation during the postionization process rather than the unimolecular fragmentation of nascent clusters in the course of the sputtering event.

With regard to the indium carbide cluster distribution, it is interesting to note that practically no InC_n clusters could be detected in the postionized neutral spectrum. However, it is possible to unambiguously identify neutral In_mC_n species with m = 2..6 containing up to n = 5 carbon atoms in the measured spectra. The abundance distributions of these clusters measured using the two different photoionization methods are plotted in Figure 5 along with those of the corresponding cationic species. Each panel depicts the progression of different numbers of carbon constituents (n) for a given number of indium atoms

dx.doi.org/10.1021/jp5024247 | J. Phys. Chem. A 2014, 118, 8542−8552

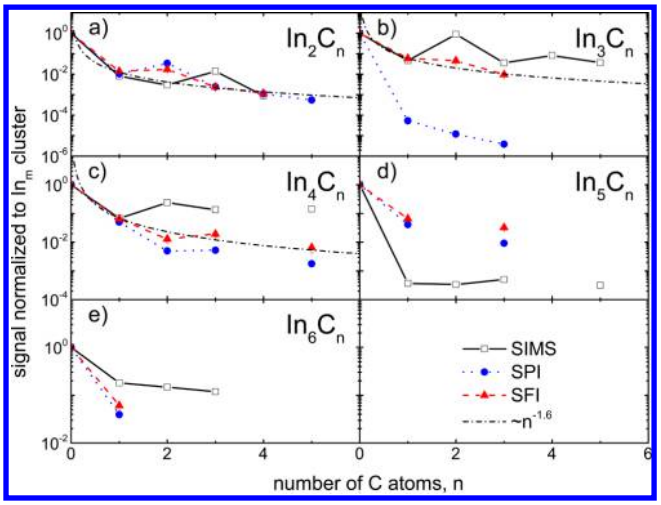

Figure 5. Size distribution of neutral (SPI, blue; SFI, red) and ionized (SIMS, black) In_mC_n clusters containing a fixed number of indium atoms produced under bombardment of solid indium with 20 keV C_{60}^+ ions. The signals were normalized to that of the respective In_m cluster.

(m) in the cluster, with each distribution being normalized to the signal of the respective pure In_m cluster. For m = 2, 4, 5 and 6, the results measured with both photoionization methods are reassuringly similar. For the case of In_3C_n clusters, on the other hand, the signal measured using VUV single photon ionization is by orders of magnitude lower than that measured using IR strong field photoionization. In this case, the missing signal must evidently be due to the photoionization process, because the SFI data clearly show that the respective neutral clusters are present in the plume. We are therefore forced to conclude that single photon ionization at 157 nm does not permit the intact photoionization of In_3C_n clusters. The most probable explanation for this observation would be that the ionization potentials of these clusters lie above the photon energy of 7.88 eV. In that case, the SPI scheme would only detect those clusters which contain enough (ionization active) internal energy to effectively lower the ionization threshold. For sputtered metal clusters, this "sub-threshold ionization" phenomenon has indeed been observed[28,44,45] and was utilized to determine the internal temperature of sputter generated indium clusters.[28] Alternatively, the signal might be caused by photofragmentation of larger clusters, most likely In_4C_n. To explain the observed linear dependence on laser intensity, however, this requires a photon energy above the sum of the ionization energy of In_4C_n plus its dissociation energy for the loss of an indium atom. The values calculated by Bernstein et al.[2] (IE = 6.5−7 eV and E_D = 2..3 eV) clearly indicate that this is not possible with a photon energy of 7.88 eV.

Looking at the calculations of Bernstein et al., one finds adiabatic ionization energies of 7.7, 5.9, and 7.1 eV for neutral In_3C, In_3C_2, and In_3C_3, respectively, which are well below our photon energy. One could argue that the threshold energy necessary for single photon ionization is rather the vertical ionization energy, which has also been calculated as 7.8, 6.6, and 7.6 eV, respectively. For In_3C and In_3C_3, these values are very close to our photon energy. Considering the possible uncertainty in the absolute values predicted by DFT calculations, the fact that we cannot observe these clusters is understandable. For In_3C_2, on the other hand, the missing signal is harder to rationalize because the calculated ionization energy is more than 1 eV below the photon energy. Therefore, either the calculated value is by more than 1 eV too low or there are other reasons like, for instance, an extremely unfavorable Franck−Condon factor which underlie our experimental finding. In this context, it should be noted that whereas the B3P86 functional used by Bernstein et al. is fine for geometry calculations, it tends to systematically *over*estimate ionization energies[b], rendering the observation of a strongly reduced SPI ionization efficiency puzzling.

Comparing the neutral cluster distributions to those of the respective secondary ions, one finds complementary trends. For the m = 2 progression, the carbide cluster ion with the highest relative abundance is $In_2C_3^+$, whereas it is In_2C_2 in the neutral spectrum. A similar observation holds for the m = 4 progression, where the $In_4C_2^+$ is the most abundant carbide ion, whereas it is In_4C in the neutral spectrum. For m = 3, the $In_3C_2^+$ ion is especially abundant (even more than the In_3^+ ion), whereas this is clearly not the case for the respective neutral clusters. For all In_mC_n clusters, the calculations[2] show that the most probable fragmentation channel, i.e., the one associated with the lowest dissociation energy, is by loss of an In atom. In that respect, a pronounced odd−even alternation is predicted[2] with all $In_3C_n^+$ cations containing an even number of carbon atoms being particularly stable, whereas this trend is reversed for the corresponding neutral clusters. This finding is consistent with our experimental data. Particularly the $In_3C_2^+$ cation exhibits the highest thresholds for all possible dissociation reactions, thus explaining the outstanding abundance of this ion in the secondary ion spectrum. Although the same holds true for the dissociation of neutral In_3C_2 via loss of C_2 and InC units, the threshold for loss of an In atom is significantly reduced with respect to In_3C and In_3C_3, thereby making the unspectacular abundance of this cluster in the neutral spectrum understandable. The general trend observed for the neutral clusters is an overall decrease of the relative abundance with increasing number n of constituent C atoms, which can roughly be approximated by an $n^{-1.6}$ dependence (dash-dotted lines in Figure 5) and is superimposed by a slight odd−even alternation reflecting the different stability of the clusters.

A different way to analyze the data is to plot the abundance distribution of In_mC_n clusters containing a fixed number of carbon atoms. These plots are shown in Figure 6. To demonstrate the relative scaling, all signals of postionized neutral clusters were normalized to that of the neutral In atom and all secondary ion signals were normalized to that of In^+. Interestingly, no carbide cluster containing only one indium atom was observed. In the remaining $m \geq 2$ progression, the neutral clusters exhibit a monotonic decrease with increasing size, i.e., number of indium atoms, which closely follows that observed for the pure indium clusters. This finding is in marked contrast with a similar experiment performed on silicon.[46] In that case, the neutral Si_mC, Si_mC_2, and Si_mC_3 clusters showed pronounced yield maxima at m = 2, 1 and 2, respectively, which could be explained by the fact that these clusters exhibit the largest dissociation threshold (i.e., the lowest dissociation energy for loss of a Si atom). In the case of indium carbide clusters, the lowest dissociation energy is the energy required for loss of an indium atom, and the calculated dissociation thresholds are significantly smaller than those of the silicon carbide clusters. Published data[2] exist only for m = 3 and 4, but there is no clear correlation with the data in Figure 6. For the cationic clusters, the most striking observation is the signal drop

dx.doi.org/10.1021/jp5024247 | J. Phys. Chem. A 2014, 118, 8542−8552

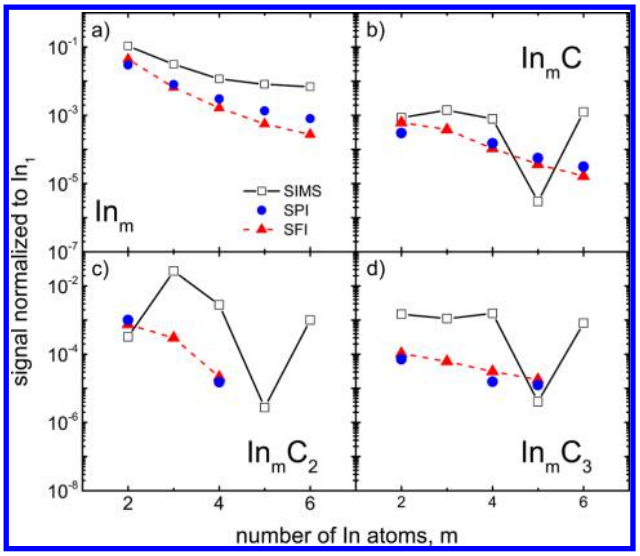

Figure 6. Size distribution of neutral (SPI, blue; SFI, red) and ionized (SIMS, black) In_mC_n clusters containing a fixed number of carbon atoms produced under bombardment of solid indium with 20 keV C_{60}^+ ions. The signals of all postionized neutrals were normalized to that of the neutral indium monomer, whereas all secondary ion signals were normalized to that of In^+.

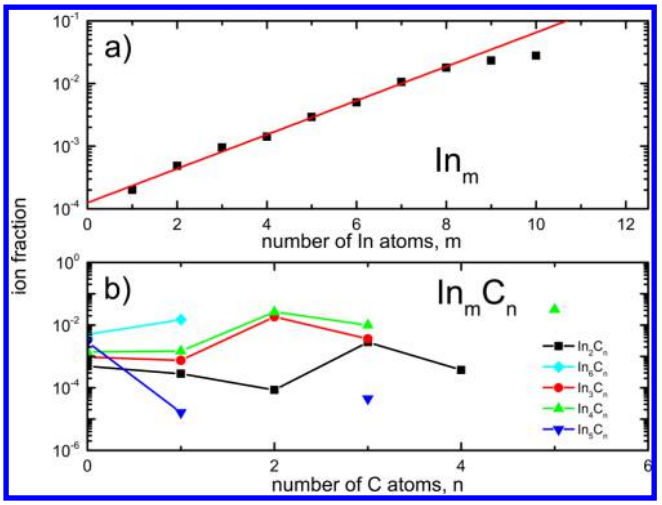

Figure 7. Ion fraction of In_m (a) and In_mC_n clusters (b) produced under bombardment of solid indium with 20 keV C_{60}^+ ions. The data were calculated using the strong field photoionization (SFI) data for postionization of the neutral species.

observed for all clusters containing 5 indium atoms. Because the neutral distributions do not show this effect, we suspect that this effect must be related to a particularly high ionization energy of the neutral In_5C_n clusters or a significantly reduced stability of the respective cluster ions. At present, this question must remain open because the corresponding threshold energies are unknown.

When comparing the relative abundance of secondary neutral and ionic clusters within the sputtered flux, one needs to keep in mind the normalization of the data presented in Figure 5. To arrive at a quantitative comparison, each $In_mC_n^+$ curve displayed in Figure 5 must be multiplied by the relative abundance of the respective In_m^+ cluster depicted in Figure 4 and the ion fraction of In^+ (2×10^{-4}) determined above. By dividing the distributions of ionized and neutral clusters, we determine the ion fraction, i.e., the probability that an In_mC_n cluster produced under C_{60} ion bombardment is formed in a cationic charge state. The result is presented in Figure 7. First, it is seen that the ion fraction is lowest for In_1 and increases with increasing number m of indium atoms in the cluster. This finding has been observed before[18] and represents a typical feature of the formation of metal clusters in sputtering, which can be rationalized at least in part by a decrease of the ionization energy with increasing cluster size. For the carbide clusters, the ion fraction exhibits a pronounced odd−even alternation with respect to the number of carbon atoms, which is similar for In_3C_n and In_4C_n but reversed for In_2C_n. For $m = 3$, this finding can be rationalized by an alternation of the calculated ionization energies, which predict smaller ionization energies for even values of n.[2] In light of the above discussion, however, caution must be used because the VUV postionization experiment suggests the IE of all three clusters with $n = 1$, 2, and 3 to be above 7.88 eV. For the $m = 4$ series, the argument does not hold because the calculated ionization energies do not show an odd−even alternation.[2] Therefore, we conclude that it is rather the stability of the produced species that governs the abundance distribution of clusters in sputtering. This is in line with the notion that sputtered clusters are formed via unimolecular fragmentation of highly internally excited "nascent" clusters.[47] In any case, it is evident that cationic species in all cases represent only a minor species in the plume of sputtered material, whereas the vast majority of particles emitted from the surface is in the neutral charge state.

Effects of C_{60} Fluence. An interesting question that was left open in the work of Bernstein et al. regards the role of carbon accumulation at the C_{60}-bombarded surface. In general, it is well-known that ion bombardment leads to the implantation of projectile constituents at or slightly below the bombarded surface. For the specific case of C_{60} bombardment, molecular dynamics (MD) simulations[48,49] as well as experimental data[46] reveal that at least part of the constituent carbon atoms are being implanted, leading to a buildup of a surface carbon concentration with increasing C_{60}^+ ion fluence, until at some point a steady state between implantation and resputtering is reached. In the context of the present work, the interesting question is to what extent the formation of sputtered In_mC_n is influenced by such an effect. In other words, are the clusters being formed in the course of a single impact event, i.e., from a combination of surface indium atoms with projectile constituents? Or, alternatively, are they being formed from C atoms already present at the surface, with the C resulting from previous C_{60} impact events? To address this question, we first investigate the mass spectra taken on a pristine indium surface that was prebombarded with a gold ion beam to such an extent that no traces of carbon were detectable any more. This surface was then analyzed with a pulsed C_{60}^+ ion beam under "static" conditions, with the C_{60}^+ ion fluence applied during data acquisition being restricted to about 2×10^{-4} ions/nm^2. With the surface area influenced by a single impact being of the order of several nm^2, each impact therefore occurs on a fresh surface location that has not been influenced by previous C_{60} bombardment, and In_mC_n clusters observed under these conditions must be formed from In and C atoms originating from the surface and the projectile, respectively. If the C_{60} fluence is increased, any change observed in the cluster yield then reflects the influence of the accumulating surface carbon concentration.

dx.doi.org/10.1021/jp5024247 | J. Phys. Chem. A 2014, 118, 8542−8552

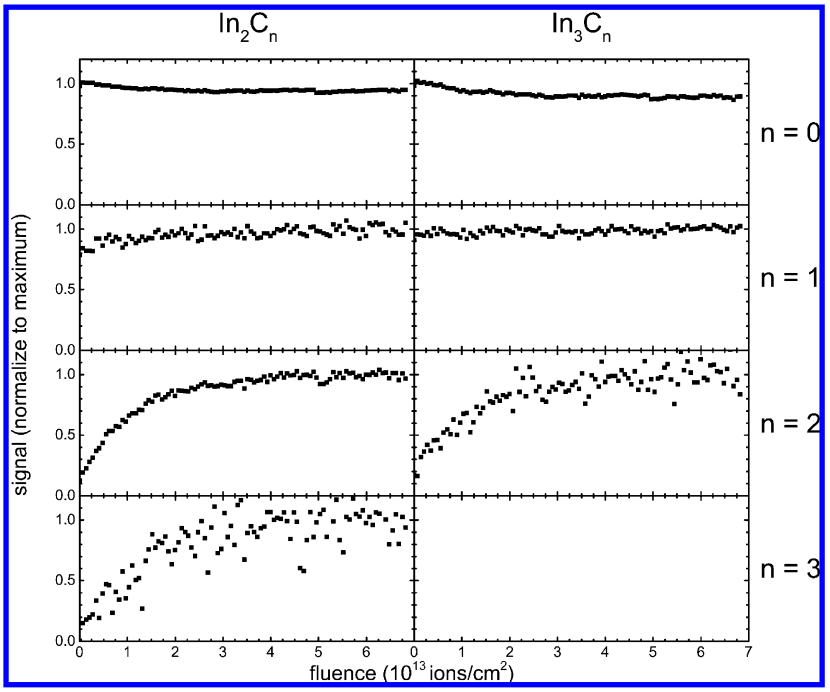

Figure 8. Yield of neutral In_2C_n and In_3C_n clusters produced under bombardment of a sputter cleaned solid indium surface with 20 keV C_{60}^+ ions vs C_{60}^+ ion fluence. The surface was prebombarded using a gold ion beam until no carbon containing clusters were detectable.

As an example of the results of such an experiment, the signals of neutral In_mC_n clusters with $m = 2$ and 3 are shown as a function of C_{60}^+ fluence in Figure 8. It is seen that two different cases can be distinguished. On one hand, clusters containing only one carbon atom exhibit a large intensity already under static conditions, which does not significantly change with increasing ion fluence. These clusters are evidently formed in single impact events, with the formation mechanism probably involving a sputtered In_m cluster picking up a carbon atom from the projectile. On the other hand, all clusters containing more than one carbon atom exhibit almost negligible intensity in the static regime, which rises to a steady state value with increasing ion fluence. At the same time, the signals of pure In_m clusters exhibit a slight decay, indicating a decreasing indium surface concentration. From this experiment, it is obvious that implanted carbon builds up at the surface, until steady state conditions are reached at an ion fluence of the order of 10^{14} C_{60}^+/cm^2. From the observed fluence dependence, we conclude that the vast majority of the In_mC_n clusters with $n > 1$ observed under steady state conditions must be formed from carbon atoms that are already present at the surface. Using a purely statistical cluster formation model, one would estimate the probability for the formation of an In_mC_n cluster to scale with the surface concentration of carbon as $c_{In}{}^m c_C{}^n$. This allows the prediction of the abundance distribution within a series of constant m once the carbon concentration is known. Applying the same scaling to the signal reduction of pure indium clusters in Figure 8, in connection with $c_{In} = (1 - c_C)$, one finds a steady state carbon concentration of the order of 5%, statistically predicting a yield variation as $In_mC:In_mC_2:In_mC_3 = 1:0.05:0.0025$. It is obvious that this strong decay with increasing n is not observed. Instead, it appears that the signal roughly follows an $n^{-\delta}$-dependence with $\delta \simeq 1.6$.

CONCLUSIONS

Complementing the data obtained for secondary cluster ions with that of the corresponding neutral clusters, it is possible to gain insight into the formation process of indium carbide clusters during C_{60} ion bombardment of solid indium. We have shown that it is possible to detect the neutral clusters using time-of-flight mass spectrometry in connection with a laser based post-ionization scheme. The quantitative interpretation of the measured data, however, hinges on the assessment of the achieved post-ionization efficiency. In the present work, we have utilized two distinctly different laser-based strategies which are both aimed at an efficient photoionization of sputtered neutral species. The obtained results demonstrate that both single photon ionization using nanosecond VUV laser pulses and strong field photoionization using extremely intense, ultrashort infrared pulses allow the efficient postionization of the sputtered indium and indium carbide clusters without excessive fragmentation. Furthermore, it is shown that the combination of both experiments is vital to identify possible problems associated with a particular method. As an example, we find that all In_3C_n clusters investigated here are practically invisible to the VUV single photon ionization, probably due to unfavorable transition probabilities or their ionization energies being above the applied photon energy. On the other hand, it is shown that the strong field photoionization scheme may significantly underestimate the abundance of neutral clusters due to the undersampling of the neutral plume with a focused laser.

If these problems are properly addressed, both postionization methods are shown to deliver nearly identical abundance distributions of the neutral In_m and In_mC_n clusters produced under C_{60}^+ ion bombardment of indium. If compared to the respective secondary ion distributions, it is demonstrated that in all cases the cationic species represent only a minor fraction of the sputtered particles. However, it is also found that the measured ion fraction significantly increases with increasing

dx.doi.org/10.1021/jp5024247 | J. Phys. Chem. A 2014, 118, 8542−8552

nuclearity, a finding which is verified for both the progression of clusters containing a constant number of In atoms and a constant number of carbon atoms, respectively. For the pure metal clusters, this finding is rather typical and can be explained at least in part by the decreasing ionization energy with increasing cluster size. For the carbide clusters, one finds an odd−even alternation of the ion fraction which can only in part be explained in terms of the calculated ionization energies.

The measured abundance of neutral In_m clusters is shown to fall monotonically with increasing m, as has been observed earlier. For In_mC_n clusters, each progression with a constant value of m shows an overall decrease with increasing number of carbon atoms according to $n^{-1.6}$, which is superimposed with an odd−even alternation reflecting the different stability of the clusters. If analyzed for constant n, the abundance also falls monotonically with increasing m. This is in marked contrast with the cation distributions, which are additionally influenced by the bombardment induced electronic excitation leading to the formation of secondary ions.

AUTHOR INFORMATION

Notes

The authors declare no competing financial interest.

ACKNOWLEDGMENTS

L.B. thanks the Deutsche Forschungsgemeinschaft for financial support in the frame of the Sonderforschungsbereich 616 “Energy dissipation at surfaces”. The authors acknowledge the financial support from the Department of Energy Grant No. DE-FG02-06ER15803.

ADDITIONAL NOTES

[a]Note that the position $y = 0$ in Figure 2 refers to a vertical distance of 500 μm between the surface and the center of the laser beam.

[b]Note that the ionization energy of In_2 calculated in ref 1 was by about 0.7 eV above the experimental value

REFERENCES

(1) Castleman, A. W.; Bowen, K. H. Clusters: Structure, Energetics, and Dynamics of Intermediate States of Matter. *J. Phys. Chem.* **1996**, *100*, 12911−12944.

(2) Bernstein, J.; Armon, E.; Zemel, E.; Kolodney, E. Formation of Indium Carbide Cluster Ions: Experimental and Computational Study. *J. Phys. Chem. A* **2013**, *117*, 11856−11865.

(3) Cohen, Y.; Bernshtein, V.; Armon, E.; Bekkerman, A.; Kolodney, E. Formation and Emission of Gold and Silver Carbide Cluster Ions in a Single C_{60}^- Surface Impact at keV Energies: Experiment and Calculations, *J. Chem. Phys.* **2011**, *134*.

(4) Blumling, D. E.; Sayres, S. G.; Castleman, A. W. Strong-Field Ionization and Dissociation Studies on Small Early Transition Metal Carbide Clusters Via Time-of-Flight Mass Spectrometry. *J. Phys. Chem. A* **2011**, *115*, 5038−5043.

(5) Knappenberger, K. L.; Jones, C. E.; Sobhy, M. A.; Iordanov, I.; Sofo, J.; Castleman, A. W. Anion Photoelectron Spectroscopy and Density Functional Investigation of Vanadium Carbide Clusters. *J. Phys. Chem. A* **2006**, *110*, 12814−12821.

(6) Stairs, J. R.; Peppernick, S. J.; Davis, K. M.; Castleman, A. W. Time-Resolved Fluence Studies and Delayed Ionization of the Niobium-Carbon Cluster System. *Isr. J. Chem.* **2004**, *44*, 223−228.

(7) Kooi, S. E.; Castleman, A. W. Delayed Ionization in Transition Metal-Carbon Clusters: Further Evidence for the Role of Thermionic Emission. *J. Chem. Phys.* **1998**, *108*, 8864−8869.

(8) Yamada, Y.; Castleman, A. W. Gas-Phase Copper Carbide Clusters. *Chem. Phys. Lett.* **1993**, *204*, 133−138.

(9) Guo, B. C.; Wei, S.; Chen, Z.; Kerns, K. P.; Purnell, J.; Buzza, S.; Castleman, A. W. Generation of Metal-Carbon and Metal-Nitrogen Clusters with a Laser-Induced Plasma Technique. *J. Chem. Phys.* **1992**, *97*, 5243−5245.

(10) Chen, Z. Y.; Guo, B. C.; May, B. D.; Cartier, S. F.; Castleman, A. W. Reaction Channels in a Plasma Reactor Laser Vaporization Source - Formation of Carbon Clusters and Metal-Carbon Clusters. *Chem. Phys. Lett.* **1992**, *198*, 118−122.

(11) Reddic, J. E.; Duncan, M. A. Composite Samples and the Generation of Novel Metal Carbide Clusters. *Chem. Phys. Lett.* **1997**, *264*, 157−162.

(12) Ticknor, B. W.; Bandyopadhyay, B.; Duncan, M. A. Photodissociation of Noble Metal-Doped Carbon Clusters. *J. Phys. Chem. A* **2008**, *112*, 12355−12366.

(13) Gibson, J. K. Laser Ablation and Gas-Phase Reactions of Small Gold Cluster Ions, Au_N^+ ($1 \le N \le 7$). *J. Vac. Sci. Technol. A* **1998**, *16*, 653−659.

(14) Wang, Y.; Szczepanski, J.; Vala, M. Silver-Carbon Cluster Agc3: Structure and Infrared Frequencies. *J. Phys. Chem. A* **2008**, *112*, 11088−11092.

(15) Szczepanski, J.; Wang, Y.; Vala, M. Copper-Carbon Cluster CuC_3: Structure, Infrared Frequencies, and Isotopic Scrambling. *J. Phys. Chem. A* **2008**, *112*, 4778−4785.

(16) Wahl, M.; Wucher, A. VUV Photoionization of Sputtered Neutral Silver Clusters. *Nucl. Instrum. Methods B* **1994**, *94*, 36−46.

(17) Wucher, A.; Wahl, M. The Formation of Clusters During Ion Induced Sputtering of Metals. *Nucl. Instrum. Methods B* **1996**, *115*, 581−589.

(18) Staudt, C.; Wucher, A. Generation of Large Indium Clusters by Sputtering. *Phys. Rev. B* **2002**, *66*, 075419−075411.

(19) Ma, Z.; Coon, S. R.; Calaway, W. F.; Pellin, M. J.; Gruen, D. M.; Nagy-Felsobuki, E. I. Sputtering of Neutral and Ionic Indium Clusters. *J. Vac. Sci. Technol.* **1994**, *12*, 2425−2430.

(20) Wucher, A.; Ma, Z.; Calaway, W. F.; Pellin, M. J. Yields of Sputtered Metal Clusters: The Influence of Surface Structure. *Surf. Sci.* **1994**, *304*, L439−L444.

(21) Coon, S. R.; Calaway, W. F.; Pellin, M. J.; White, J. M. New Findings on the Sputtering of Neutral Metal Clusters. *Surf. Sci.* **1993**, *298*, 161−172.

(22) Coon, S. R.; Calaway, W. F.; Burnett, J. W.; Pellin, M. J.; Gruen, D. M.; Spiegel, D. R.; White, J. M. Yields and Kinetic Energy Distributions of Sputtered Neutral Copper Clusters. *Surf. Sci.* **1991**, *259*, 275−287.

(23) Levis, R. J.; Dewitt, M. J. Photoexcitation, Ionization, and Dissociation of Molecules Using Intense near-Infrared Radiation of Femtosecond Duration. *J. Phys. Chem. A* **1999**, *103*, 6493−6507.

(24) Kucher, A.; Wucher, A.; Winograd, N. Strong Field Photoionization of B-Estradiol between 1200 Nm and 2000 Nm: Strategies to Optimize Molecular Post-Ionization in Secondary Neutral Mass Spectrometry. *Anal. Chem.*, submitted for publication.

(25) Kucher, A.; Jackson, L. M.; Lerach, J. O.; Bloom, A. N.; Popczun, N. J.; Wucher, A.; Winograd, N. Strong Field Ionization and Imaging of C_{60} Sputtered Molecules: Overcoming Matrix Effects and Improving Sensitivity.*Anal. Chem.*, submitted for publication

(26) Braun, R. M.; Blenkinsopp, P.; Mullock, S. J.; Corlett, C.; Willey, K. F.; Vickerman, J. C.; Winograd, N. Performance Characteristics of a Chemical Imaging Time-of-Flight Mass Spectrometer. *Rapid Commun. Mass Spectrom.* **1998**, *12*, 1246−1252.

(27) Mazarov, P.; Samartsev, A.; Wucher, A. Determination of Energy Dependent Ionization Probabilities of Sputtered Particles. *Appl. Surf. Sci.* **2006**, *252*, 6452−6455.

(28) Wucher, A.; Staudt, C.; Neukermans, S.; Janssens, E.; Vanhoutte, F.; Silverans, R. E.; Lievens, P. On the Internal Energy of Sputtered Clusters. *New. J. Phys.* **2008**, *10*, 1−22.

(29) Baguenard, B.; Pellarin, M.; Bordas, C.; Lerme, J.; Vialle, J. L.; Broyer, M. Shell Structure of Small Indium Clusters Below N =200 Atoms. *Chem. Phys. Lett.* **1993**, *205*, 13−18.

(30) Koch, D.; Wahl, M.; Wucher, A. Electron Impact and Single Photon Ionization Cross Sections of Neutral Silver Clusters. *Z. Phys. D* **1994**, *32*, 137−144.
(31) Wucher, A. Laser Postionization - Fundamentals. In *Tof-Sims: Materials Analysis by Mass Spectrometry*, 2nd ed.; Vickerman, J. C., Briggs, D., Eds.; IM Publications: Chichester, U.K., 2013; pp 217 - 246.
(32) Wucher, A. Formation of Clusters in Sputtering. *Izv. Akad. Nauk, Ser. Fiz.* **2002**, *66*, 499−508.
(33) Hankin, S. M.; Villeneuve, D. M.; Corkum, P. B.; Rayner, D. M. Intense-Field Laser Ionization Rates in Atoms and Molecules. *Phys. Rev. A* **2001**, *64*, 013405−013412.
(34) Postawa, Z. Personal communication.
(35) Samartsev, A. V.; Heuser, C.; Wucher, A. Ionization Probabilities of Sputtered Indium Atoms under Atomic and Polyatomic Au_m- Ion Bombardment. *Surf. Interface Anal.* **2012**, *45*, 87−89.
(36) Coon, S. R.; Calaway, W. F.; Pellin, M. J. Neutral Copper Cluster Sputtering Yields: Ne^+, Ar^+ and Xe^+ Bombardment. *Nucl. Instrum. Methods B* **1994**, *90*, 518−522.
(37) Wucher, A. Sputtering: Experiment. *Kgl. Dansk. Vid. Selsk. Mater. Fys. Medd.* **2007**, *52*, 405−432.
(38) King, B. V.; Veryovkin, I. V.; Moore, J. F.; Calaway, W. F.; Pellin, M. J. Formation of Neutral Clusters During Sputtering of Gold. *Surf. Sci.* **2009**, *603*, 819−825.
(39) Staudt, C.; Heinrich, R.; Wucher, A. Formation of Large Clusters During Sputtering of Silver. *Nucl. Instrum. Methods B* **2000**, *164−165*, 677−686.
(40) Heinrich, R.; Wucher, A. Projectile Size Effects on Cluster Formation in Sputtering. *Nucl. Instrum. Methods B* **2003**, *207*, 136−144.
(41) Heinrich, R.; Wucher, A. Cluster Formation under Bombardment with Polyatomic Projectiles. *Nucl. Instrum. Methods B* **2000**, *164−165*, 720−726.
(42) Sigmund, P.; Claussen, C. Sputtering from Elastic-Collision Spikes in Heavy-Ion-Bombarded Metals. *J. Appl. Phys.* **1981**, *52*, 990−993.
(43) Sun, S.; Szakal, C.; Winograd, N.; Wucher, A. Energetic Ion Bombardment of Ag Surfaces with C_{60}^+ and Ga^+ Projectiles. *J. Am. Soc. Mass Spectrom.* **2005**, *16*, 1677−1686.
(44) Wucher, A. Internal Energy of Sputtered Metal Clusters. *Phys. Rev. B* **1994**, *49*, 2012−2020.
(45) Takahashi, L. K.; Zhou, J.; Wilson, K. R.; Leone, S. R.; Ahmed, M. Imaging with Mass Spectrometry: A Secondary Ion and VUV-Photoionization Study of Ion-Sputtered Atoms and Clusters from GaAs and Au. *J. Phys. Chem. A* **2009**, *113*, 4035−4044.
(46) Wucher, A.; Kucher, A.; Winograd, N.; Briner, C. A.; Krantzman, K. D. Sputtered Neutral Sincm Clusters as a Monitor for Carbon Implantation During C_{60} Bombardment of Silicon. *Nucl. Instrum. Methods B* **2011**, *269*, 1300−1305.
(47) Wucher, A.; Garrison, B. J. Unimolecular Decomposition in the Sputtering of Metal Clusters. *Phys. Rev. B* **1992**, *46*, 4855−4864.
(48) Krantzman, K. D.; Garrison, B. J. Molecular Dynamics Simulations to Explore the Effect of Chemical Bonding in the keV Bombardment of Si with C_{60}, Ne_{60} and $^{12}Ne_{60}$) Projectiles. *Nucl. Instrum. Methods B* **2009**, *267*, 652−655.
(49) Krantzman, K. D.; Briner, C. A.; Garrison, B. J. Investigation of Carbon Buildup in Simulations of Multi-Impact Bombardment of Si with 20 keV C_{60} Projectiles. *J. Phys. Chem. A* **2014**, DOI: 10.1021/jp4108624.